



## Full Text View

[Volume 29, Issue 9 \(September 1999\)](#)

### Journal of Physical Oceanography

Article: pp. 2266–2284 | [Abstract](#) | [PDF \(252K\)](#)

# Impact of Interbasin Exchange on the Atlantic Overturning Circulation

**Wilbert Weijer, Wilhelmus P. M. de Ruijter, Henk A. Dijkstra, and Peter Jan van Leeuwen**

*Institute for Marine and Atmospheric Research Utrecht, Utrecht University, Utrecht, Netherlands*

(Manuscript received October 29, 1997, in final form October 14, 1998)

DOI: 10.1175/1520-0485(1999)029<2266:IOIEOT>2.0.CO;2

### ABSTRACT

The thermohaline exchange between the Atlantic and the Southern Ocean is analyzed, using a dataset based on WOCE hydrographic data. It is shown that the salt and heat transports brought about by the South Atlantic subtropical gyre play an essential role in the Atlantic heat and salt budgets. It is found that on average the exported North Atlantic Deep Water (NADW) is fresher than the return flows (basically composed of thermocline and intermediate water), indicating that the overturning circulation (OC) *exports* freshwater from the Atlantic.

The sensitivity of the OC to interbasin fluxes of heat and salt is studied in a 2D model, representing the Atlantic between 60°N and 30°S. The model is forced by mixed boundary conditions at the surface, and by realistic fluxes of heat and salt at its 30°S boundary. The model circulation turns out to be very sensitive to *net* buoyancy fluxes through the surface. Both net surface cooling and net surface saltening are sources of potential energy and impact positively on the circulation strength. The vertical distributions of the lateral fluxes tend to stabilize the stratification, and, as they extract potential energy from the system, tend to weaken the flow. These results imply that a change in the composition of the NADW return transports, whether by a change in the ratio thermocline/intermediate water, or by a change in their thermohaline characteristics, might influence the Atlantic OC considerably.

It is also shown that the circulation is much more sensitive to changes in the shape of the lateral buoyancy flux than to changes in the shape of the surface buoyancy flux, as the latter does not explicitly impact on the potential energy of the system. It is concluded that interocean fluxes of heat and salt are important for the strength and operation of the Atlantic thermohaline circulation, and should be correctly represented in models that are used for climate sensitivity studies.

#### Table of Contents:

- [Introduction](#)
- [Fluxes of heat and salt](#)
- [The model](#)
- [Impact of lateral fluxes](#)
- [Discussion](#)
- [Summary and conclusions](#)
- [REFERENCES](#)
- [APPENDIX](#)
- [TABLES](#)
- [FIGURES](#)

#### Options:

- [Create Reference](#)
- [Email this Article](#)
- [Add to MyArchive](#)
- [View Correction to this Article](#)
- [Search AMS Glossary](#)

#### Search CrossRef for:

- [Articles Citing This Article](#)

#### Search Google Scholar for:

- [Wilbert Weijer](#)
- [Wilhelmus P. M. de Ruijter](#)
- [Henk A. Dijkstra](#)
- [Peter Jan van Leeuwen](#)

## 1. Introduction

The operation and the stability of the ocean global thermohaline circulation are currently receiving a great deal of attention. The interest has arisen through the realization that the ocean is an extremely important component in the climate system and that it might have played an important role in dramatic climatic events during the last ice age (e.g., [Broecker et al. 1985](#); [Keigwin et al. 1991](#)). Concern with global warming due to anthropogenic influences has increased public and scientific interest in the stability of the oceanic component of the climate system.

An appealing account of how this so-called conveyor belt circulation operates was given by [Broecker \(1991\)](#). He portrays the overturning circulation as a self-sustained circulation loop, which is driven by atmospheric freshwater transport from the Atlantic drainage basin to the Pacific. This export of freshwater is brought about by relatively high surface water temperatures, which cause evaporation to exceed precipitation in the Atlantic Ocean (e.g., [Wijffels et al. 1992](#)). These high temperatures are established by anomalous northward heat transport in the southern part of the Atlantic Ocean, which is a manifestation of the large impact of the conveyor belt circulation. The high Atlantic surface salinities allow the surface water masses to be converted into a dense deep water mass when they are cooled at high latitudes. According to this view the excess salt, which remains when net freshwater is distilled from the Atlantic surface waters, is removed by the lower limb of the conveyor belt and exported with the North Atlantic Deep Water (NADW). A two-dimensional modeling study ([Zaucker et al. 1994](#)) does indeed display a positive relation between the atmospheric freshwater loss from the Atlantic and the overturning strength.

The upper-level water masses, which enter the Atlantic to compensate for this outflow of NADW, are derived from basically two sources. They contribute water with highly contrasting water mass characteristics ([Schmitz 1995](#)): probably the largest part of the NADW compensation is derived from relatively fresh and cold intermediate waters, which enter the Atlantic as part of the Antarctic Circumpolar Circulation (ACC) through Drake Passage ([Broecker 1991](#); [Rintoul 1991](#)). The remaining part is derived from warm and salty thermocline or central water masses ([Gordon 1985, 1986](#)), which enter the Atlantic around the Cape of Good Hope by the process of “Agulhas Leakage” ([Lutjeharms 1996](#); [De Ruijter et al. 1999](#)). However, previous budget calculations ([Stommel 1980](#); [Piola and Gordon 1986](#)) failed to reconcile reasonable volume transports of NADW and thermocline and intermediate water return transports with net evaporation from the Atlantic basin.

In a recent paper, [Rahmstorf \(1996\)](#) disputes the view of [Broecker \(1991\)](#). On the basis of a series of global model experiments, he suggests that the average salinity of the water exported from the Atlantic (NADW) is *lower* than that of the water masses that replace it. This indicates that the overturning circulation *gains* freshwater on its way through the Atlantic, by an amount that is called the “active” freshwater flux by Rahmstorf. This active freshwater flux is determined by the saline characteristics of the exported NADW and the returning upper-level water masses. It is clear that the overturning circulation does not supply the freshwater for the excess Atlantic evaporation as proposed by Broecker, as it exports freshwater itself. [Rahmstorf \(1996\)](#) argues that only the wind-driven circulation of the South Atlantic subtropical gyre might import enough freshwater to reconcile the evaporative freshwater loss and the net freshwater gain of the overturning circulation. The zonal salinity contrast at 30°S in the South Atlantic Ocean does indeed exceed 1.5 psu ([Levitus 1982](#)), the highest salinities coinciding with the southward flowing Brazil Current and the lowest with the northward flowing Benguela Current. The large contribution of the gyre-induced salt transport might resolve the inconsistencies encountered in the earlier budget calculations since the overturning circulation is now released from the constraint of having to balance the atmospheric freshwater loss.

Not only are the NADW return transports important for the net interbasin fluxes of heat and freshwater, they might also affect the circulation strength in a more direct way. [Gordon et al. \(1992\)](#) suggest that the input of salty and warm thermocline water by the process of Agulhas leakage preconditions the Atlantic for forming deep water. Besides excess evaporation, this process could be an additional reason for the high surface salinities in the North Atlantic. This idea is especially interesting in view of the highly intermittent character of Agulhas leakage, and that it exists due to coupling of the wind-driven subtropical gyres of the south Indian and Atlantic Oceans ([De Ruijter 1982](#); [Lutjeharms 1996](#); [De Ruijter et al. 1998](#)). The input of warm and salty water from the Pacific and Indian Oceans into the Atlantic therefore depends critically on characteristics of the Indian Ocean wind stress fields, and this exchange might be very sensitive to climatological shifts of latitudes of zero wind stress curl. Paleoceanographic data indicate large shifts in the latitudinal positions of the major fronts in the Indian Ocean ([Howard and Prell 1992](#)), and suggest that the present-day position of the subtropical convergence, which might be thought of as the southern edge of the wind-driven subtropical gyres, is several degrees south of the average position over the last 500 kyr.

[Cai and Greatbatch \(1995\)](#) have considered the suggestion of [Gordon et al. \(1992\)](#) by comparing the overturning strength with and without Agulhas leakage in a low-resolution ocean model. In their model the overturning strength did not change in response to shutting off the Agulhas leakage. They blame this lack of response on the hardly changed density field, as thermal and saline changes almost canceled each other out. [Rahmstorf et al. \(1996\)](#) suggest that this might have been due to an inappropriately weak thermal coupling to the atmosphere, allowing thermal anomalies to affect the density throughout the

basin, instead of in the South Atlantic only. Nevertheless it remains unclear why the *overturning* does not change in response to shutting off Agulhas leakage, despite considerable changes in several other thermohaline properties of the solution.

In this paper we examine how the strength and the operation of the Atlantic overturning circulation are influenced by interbasin fluxes of heat and salt. We demonstrate that not only the *net* flux of buoyancy across 30°S in the Atlantic is relevant, but the *vertical distribution* of the lateral buoyancy exchange as well. This distribution is a result of the highly distinct thermal and saline characteristics of the exported NADW and the brands of imported shallow-level water. We show that the vertical structure of the lateral buoyancy flux can have a larger impact on the overturning strength than its influence on surface salinities and deep convection alone: it directly modifies the balance of potential energy of the Atlantic Ocean and hence the overturning strength. Modification of this vertical distribution, by changing the thermal or saline characteristics of the water masses (e.g., by changing the amount of Agulhas inflow) or by changing the vertical structure of the overturning (e.g., by changing the ratio of thermocline to intermediate water in the compensation), might therefore induce changes in the overturning strength.

The aim of this paper is to clarify the relative role played by lateral and surface buoyancy fluxes in the operation of the large-scale Atlantic overturning circulation in a simple model context. It is essential to determine the importance of both lateral and surface forcing in order to understand and predict the ocean's response to climatic changes. Given the observed variability of Agulhas leakage and its sensitivity to characteristics of the wind stress fields in the Indian Ocean, this question is highly relevant for climate studies. It is also important for judging the skill of low and high resolution ocean models, which do not incorporate Agulhas leakage (Drijfhout et al. 1996) or fail to reproduce the formation of intermediate water correctly (McCann et al. 1994). It is furthermore relevant for judging the applicability of two-dimensional models of the overturning circulation, which lack the zonal dimension and the associated transport mechanism of the wind-driven circulation (e.g., Zaucker et al. 1994).

In [section 2](#) of this paper, zonally averaged profiles will be presented of fluxes of heat and salt across 30°S in the Atlantic. These estimates are based on an inversion of several hydrographic datasets from the South Atlantic, including some recent sections from the World Ocean Circulation Experiment (WOCE). In [section 3](#), we describe the simple 2D model of the Atlantic Ocean employed for this study, which is forced by realistic surface and lateral fluxes, the latter being parameterized as diffusive fluxes. In [section 4](#) the impact of these fluxes on the overturning strength is studied. The relevance and implications of these results are discussed in [section 5](#), and the main conclusions are summarized in [section 6](#).

## 2. Fluxes of heat and salt across 30°S

In this section we present zonally averaged profiles of advective fluxes of heat and salt across 30°S in the Atlantic Ocean. These fluxes represent the thermal and saline coupling between the Atlantic and Southern Oceans, as they account for the interocean exchange of heat and salt via the ocean. They were calculated using the “best estimate” solution of an inversion discussed by [Holfort \(1994\)](#). He combined hydrographic data from several South Atlantic WOCE sections and some earlier cruises to obtain a best estimate of the balances of mass, salt, and heat in the South Atlantic. In the following we will use the meridional mass flux  $\mathbf{v}_m = \rho \mathbf{v}$  (in  $\text{kg m}^{-2} \text{s}^{-1}$ ) rather than the meridional velocity  $\mathbf{v}$  itself.

Denoting the longitude by  $\phi$  and depth by  $z$ , we split the meridional mass flux  $\mathbf{v}_m(\phi, z)$ , potential temperature  $T(\phi, z)$ , and salinity  $S(\phi, z)$  at this section into a zonal mean and its deviation; that is,

$$\begin{aligned} T(\phi, z) &= \bar{T}(z) + T'(\phi, z) \\ S(\phi, z) &= \bar{S}(z) + S'(\phi, z) \\ \mathbf{v}_m(\phi, z) &= \bar{\mathbf{v}}_m(z) + \mathbf{v}'_m(\phi, z), \end{aligned} \quad (1)$$

where

$$(\bar{T}(z), \bar{S}(z), \bar{\mathbf{v}}_m(z)) \equiv \frac{1}{L(z)} (\overline{T(\phi, z)}, \overline{S(\phi, z)}, \overline{\mathbf{v}_m(\phi, z)}) \quad (2)$$

and

$$(\overline{T'(\phi, z)}, \overline{S'(\phi, z)}, \overline{\mathbf{v}'_m(\phi, z)}) = 0. \quad (3)$$


Here  $L(z)$  is the width of the basin at depth  $z$ , and the overbars denote zonal integration (note that  $\bar{T}$ ,  $\bar{S}$ , and  $\bar{\mathbf{v}}_m$  are zonal


means). To calculate heat and salt transports we introduce a reference temperature  $T_0$  and a reference salinity  $S_0$ ; the appropriate choices for  $T_0$  and  $S_0$  will be discussed later. The zonally averaged lateral fluxes of heat and salt are given by



$$\begin{aligned} F_Q(z) &= \frac{1}{L(0)} c_p \overline{v_m (T - T_0)} \\ &= \frac{L(z)}{L(0)} c_p \overline{v_m} (\bar{T} - T_0) + \frac{1}{L(0)} c_p \overline{v'_m T'} \end{aligned} \quad (4a)$$

$$\begin{aligned} F_S(z) &= \frac{1}{L(0)} \overline{v_m (S - S_0)} \\ &= \frac{L(z)}{L(0)} \overline{v_m} (\bar{S} - S_0) + \frac{1}{L(0)} \overline{v'_m S'}. \end{aligned} \quad (4b)$$

Applying the factor  $L(0)$  in the averaging procedure yields a depth-dependent weight factor  $L(z)/L(0)$ , which is the relative width of the basin at each depth. This places the fluxes in the deeper and narrower parts of the basin in the right proportions with respect to their shallower counterparts. The first terms on the right-hand sides of Eqs. (4) denote heat and salt fluxes brought about by the overturning circulation, the net meridional transport at each depth advecting the zonally averaged temperature and salinity deviation. The second terms denote the contributions of the (largely horizontal) gyre circulation, and arise when velocity anomalies correlate with deviations of the thermal or saline anomalies within a layer.

It is not clear a priori what values of  $T_0$  and  $S_0$  should be taken since every reference state yields an equally valid description of the fluxes. In appendix A it is shown that, in the context of our model, the appropriate choice for  $T_0$  and  $S_0$  is the averaged value of temperature and salinity in the basin. Only then is the potential energy input of these fluxes into the Atlantic correctly captured in our model. Using the [Levitus \(1982\)](#) dataset, we averaged the temperature and salinity for the Atlantic Ocean (including the Mediterranean), starting at 30°S and going up to the Labrador Sea and the North Atlantic overflow ridges resulting in mean values  $T_0 = 4.83^\circ\text{C}$  and  $S_0 = 35.07$  psu. An indication of the sensitivity of these values to the exact position of the northern boundary was obtained by changing this position between 60° and 70°N, displaying variations in temperature of 0.04 K and of 0.003 psu in salinity per 10° lat. These variations do not significantly change the flux profiles. The heat capacity  $c_p$  is taken to be 4000 J kg<sup>-1</sup> K<sup>-1</sup> ([Table 1](#) ) .

The profiles of the total fluxes of heat and salt (solid lines), the overturning components (long-dashed lines), and the residual components (short-dashed lines) are plotted in [Fig. 1](#)  . The characteristics of the major water masses can be recognized in the overturning components of both heat and salt fluxes. The signal of Antarctic Bottom Water (AABW) is visible below the zero-crossings of the profiles at about 3450-m depth. It is characterized by the export of heat and salt due to northward transport of water that is fresher and colder than the average Atlantic waters. The influence of NADW is visible between the zero-crossings at about 1150 and 3450 m. Due to its relatively low salinity and temperature, the southward flow of this water mass implies *northward* fluxes of heat and salt. In the overturning salt flux, the low-salinity intermediate water is visible between 500 and 1150 m. Here the salt flux is southward due to the net northward transport of this relatively fresh water mass. The overturning fluxes in the thermocline layer are characterized by strong northward transports of heat and salt.

The residual components of the heat and salt fluxes are very small below the upper kilometer: zonal variations in the thermohaline structure are small at these depths, and the horizontal circulation is weak. Here, the total fluxes are controlled by the overturning components alone. Above these depths the residual fluxes of heat and salt become increasingly important. Here the circulation is dominated by the wind-driven circulation of the subtropical gyre, and the zonal differences in temperature and salinity can be as much as 6°C and 1.5 psu between the eastern and western South Atlantic surface waters. [Figure 1a](#)  shows that in the upper 1000 m the northward heat flux is strongly counteracted by the residual component. In an integrated sense, the residual heat flux accounts for a 0.37 PW reduction in the 0.63 PW overturning heat flux, resulting in a total heat flux of 0.26 PW. The residual salt flux, on the other hand, completely overrules the overturning component in the upper kilometer and becomes the dominant factor in the total salt flux ([Fig. 1b](#) ). It converts the 7.0 Gg s<sup>-1</sup> *northward* salt transport of the overturning circulation into a 6.2 Gg s<sup>-1</sup> *southward* transport. [Note that the original solution of Holfort also accounts for fluxes brought about by (southward) Ekman flow and that taking  $T_0$  and  $S_0$  close to the 30°S section-mean values of temperature and salinity suppresses the heat and salt flux contribution of advection by the  $O$  (−0.3 Sv) net Atlantic volume flux.]

The sign of the salt flux at NADW levels depends of course on the choice of the reference salinity  $S_0$ . However, the sign of the integral of the overturning profile does not. Its positive sign confirms the ideas of [Rahmstorf \(1996\)](#), namely, that at 30°S the exported NADW is on average fresher than the water masses that replace it. Therefore, the overturning circulation effectively *exports* freshwater from the Atlantic and is unable to supply freshwater to compensate for the excess evaporation ([Broecker 1991](#)). The analysis of the heat and salt fluxes across 30°S in the Atlantic clearly shows the importance of the wind-driven circulation for both the heat and salt budgets of the Atlantic Ocean.

### 3. The model

#### a. Domain and configuration

The model used in this study is adapted from the two-dimensional model used by [Dijkstra and Molemaker \(1997\)](#). The stationary and rotationless Boussinesq equations are solved in a streamfunction–vorticity formulation, in a small aspect ratio configuration. Two different domain configurations are studied: the first one considers a model with equatorially symmetric surface buoyancy forcing. This model, which will be denoted as “global,” has been studied by several authors in as many parameter settings ([Cessi and Young 1992](#); [Thual and McWilliams 1992](#); [Quon and Ghil 1992, 1995](#); [Dijkstra and Molemaker 1997](#)). The second configuration, called “Atlantic,” applies more specifically to the Atlantic Ocean, which we consider bounded by the 30°S parallel. In both cases the model coordinate  $y$  ( $\in[0, 1]$ ) can be mapped onto the latitude  $\theta$ :

$$\theta_q(y) = \theta_q^S(1 - y) + \theta_q^N y \quad q = G, A, (5)$$

where  $\theta^N$  is 60, and  $\theta^S$  is  $-60$  for the global ( $G$ ) configuration and  $-30$  for the Atlantic ( $A$ ) configuration.

In addition to being forced by surface forcing, the Atlantic configuration of the model can also be forced by *lateral* fluxes of heat and salt, prescribed at the 30°S boundary. In reality, such lateral fluxes are a result of water mass exchange with anomalous salt and heat content, and are therefore of an advective nature. However, in order to avoid open boundary conditions at the southern boundary of our model, we prescribe them as diffusive fluxes, in combination with a no-flow condition. We realize that, by prescribing these fluxes, no feedback from changing Atlantic overturning to these fluxes is allowed. Furthermore the constraint that all deep water must upwell north of 30°S is an unrealistic feature of the model, as most of the NADW produced is exported from the Atlantic ([Schmitz 1995](#)).

#### b. Equations and scaling

Scale parameters and dimensionless quantities introduced in this section are tabulated in [Table 1](#), as well as their characteristic values. Dimensional variables are indicated with an \*.

A linear equation of state is used, relating buoyancy  $B^*$  to temperature  $T^*$  and salinity  $S^*$  via  $B^* = \rho_0[\alpha(T^* - T_0) - \beta(S^* - S_0)]$ . Here  $\alpha$  and  $\beta$  are the coefficients of thermal and saline expansion, and  $T_0$  and  $S_0$  are reference values of temperature and salinity. The temperature and salinity deviations are scaled with characteristic scales of thermal and saline variations in the Atlantic Ocean  $\Delta T$  and  $\Delta S$ . Scaling buoyancy  $B^*$  with  $\rho_0\alpha\Delta T$  yields  $B = T - \lambda S$ . As in [Dijkstra and Molemaker \(1997\)](#), we rescale salinity with the buoyancy ratio  $\lambda = \beta\Delta S/\alpha\Delta T$  by introducing  $\tilde{S} = \lambda S$ . The tilde will be dropped in the following.

The meridional and depth coordinates of the basin are scaled as  $(y^*, z^*) = [Ly, H(z - 1)]$ , where  $H$  is the depth scale of the basin and  $L$  the meridional extent. Coefficients of viscosity and thermal diffusivity are denoted by  $\nu$  and  $\kappa$ , respectively, with subscripts  $h$  and  $\mathbf{v}$  indicating the horizontal and vertical components. Time  $t^*$ , streamfunction  $\Psi^*$ , and vorticity  $\Omega^*$  are scaled with  $H^2/\kappa_{\mathbf{v}}$ ,  $\kappa_{\mathbf{v}}L/H$ , and  $\kappa_{\mathbf{v}}L/H^3$ . Applying this scaling, we obtain the following equations:

$$\text{Le} \left[ \frac{\partial S}{\partial t} - J(\psi, S) \right] = a^2 \frac{\kappa_h}{\kappa_v} S_{yy} + S_{zz}, \quad (6d)$$

where  $J(a, b)$  denotes the Jacobian operator  $a_y b_z - a_z b_y$ . The Prandtl number  $\text{Pr} = \nu_{\mathbf{v}}/\kappa_{\mathbf{v}}$  is taken to be 2.25, in line with the [Dijkstra and Molemaker \(1997\)](#) and [Quon and Ghil \(1992\)](#) values, whereas the aspect ratio  $a = H/L$  is taken to be  $5 \times 10^{-4}$ . The Lewis number,  $\text{Le}$ , which is the ratio between eddy diffusivities of salinity and temperature, is taken to be unity since turbulent mixing of salt and temperature is assumed to take place at the same rate.

Estimates of the Rayleigh number  $\text{Ra} = ag\Delta TH^5/\nu_{\mathbf{v}}\kappa_{\mathbf{v}}L^2$  based on realistic parameter values ([Table 1](#)) are  $O(10^{10-11})$ . However, applying a Rayleigh number of this order of magnitude would result in an unrealistically strong overturning circulation as rotational effects are not included in our model. The presence of rotation tends to stabilize a convective system, as pressure forces are not balanced by viscous friction, as in our model, but by the Coriolis force. This effectively reduces the Rayleigh number by a factor  $\text{Ta}^{-1}$ , where  $\text{Ta}$  is some kind of Taylor number, being proportional to the square of the Coriolis parameter [e.g., [Chandrasekhar 1961](#); [Van der Schrier and Maas 1998](#), their Eq. (17g)]. In this study  $\text{Ra}$  is given the low value of  $10^4$ , to enable the performance of calculations on grids with a manageable resolution. Furthermore, it has been shown ([Dijkstra and Molemaker 1997](#)) that the qualitative behavior of the system is not very sensitive to  $\text{Ra}$ , once its value is large enough.

As argued by [Quon and Ghil \(1995\)](#), small aspect ratio geophysical fluid systems can only be advective when the ratio of vertical and horizontal diffusivities (and viscosities) is also very small. Estimates of these parameters in the real ocean are of the order of  $10^{-4}$  and  $10^3 \text{ m}^2 \text{ s}^{-1}$  for  $\kappa_{\mathbf{v}}$  and  $\kappa_h$ , respectively. This yields a ratio  $\kappa_{\mathbf{v}}/\kappa_h$  of the order  $10^{-7}$ , which is of the same order of magnitude as  $a^2$ . So by taking the ratios  $\kappa_{\mathbf{v}}/\kappa_h$  and  $\nu_{\mathbf{v}}/\nu_h$  equal to  $a^2$ , we place our model in the advective regime. From Eqs. (6) it is clear that the dimensionless vertical and horizontal diffusive transports are now of the same order of magnitude.

### c. Boundary conditions

Let  $\Gamma$  denote the boundary of the domain and  $\mathbf{n}$  its outward normal, and let subscripts  $s$ ,  $r$ ,  $b$ , and  $l$  refer to the surface, right (northern), bottom, and left (southern) sides of the domain. We prescribe all walls to be free slip:

$$\psi = \Omega = 0 \quad \text{for } \mathbf{x} \in \Gamma. \quad (7a)$$

The boundary conditions for temperature are

$$\begin{aligned} T &= T_s(y) & \text{for } \mathbf{x} \in \Gamma_s \\ \nabla T \cdot \mathbf{n} &= \begin{cases} \tau_l F_l^T(z) & \text{for } \mathbf{x} \in \Gamma_l \\ 0 & \text{for } \mathbf{x} \in \Gamma_r, \Gamma_b \end{cases} \end{aligned} \quad (7b)$$

and for salinity

$$\nabla S \cdot \mathbf{n} = \begin{cases} -\sigma_s F_s^S(y) & \text{for } \mathbf{x} \in \Gamma_s \\ \sigma_l F_l^S(z) & \text{for } \mathbf{x} \in \Gamma_l \\ 0 & \text{for } \mathbf{x} \in \Gamma_r, \Gamma_b \end{cases} \quad (7c)$$

where the amplitudes  $\tau_l$ ,  $\sigma_l$ , and  $\sigma_s$  are parameters of the system, and where  $F_l^T(z)$ ,  $F_l^S(z)$ , and  $F_s^S(y)$  are  $O(1)$  functions that will be derived in the following sections.

#### 1) SURFACE FORCING

The zonally averaged profile of Atlantic Ocean surface temperatures ([Levitus 1982](#)) can be modeled reasonably well by a

cosine function of the form:

$$T_s(y) = \cos\left(\frac{\pi}{60}\theta(y)\right), \quad (8)$$

where the mapping  $\theta(y)$  is given by [Eq. \(5\)](#). This profile of prescribed temperature  $T_s$  is plotted in [Fig. 2](#) (solid line).

Three estimates of the surface freshwater flux over the Atlantic Ocean, which is equal to the difference between precipitation, runoff, and evaporation (denoted  $P - E$  for convenience), are shown in [Fig. 3](#). [Zaucker et al. \(1994\)](#) derived the profiles from ECMWF data (dashed line) and from the [Oort \(1983\)](#) climatology (dashed-dotted line) assuming that the volumes of freshwater apply to a  $60^\circ$  wide ocean basin, in order to obtain units of  $\text{m}^3 \text{m}^{-2} \text{s}^{-1}$ . The solid line was obtained from the [Baumgartner and Reichel \(1975\)](#) dataset by making the same assumption. Although the three profiles differ in detail, they agree on the particular form of the  $P - E$  profiles in the Atlantic basin: they all show excess precipitation at high latitudes, excess evaporation at midlatitudes, and a high precipitative maximum over equatorial regions, at latitudes of the intertropical convergence zone. In many 2D studies of the global thermohaline circulation, this precipitative maximum has not been taken into account, although it constitutes a considerable input of freshwater and may have a considerable impact on the stability and structure of possible overturning states.

We averaged the three profiles and symmetrized the result with respect to the equator. A simple analytical function was fitted through this profile  $\hat{F}_s^S(\theta)$  between  $60^\circ\text{S}$  and  $60^\circ\text{N}$ , yielding an  $O(1)$  profile  $F_s^S(y)$  and an amplitude  $A = 33.1 \times 10^{-9} \text{ m s}^{-1}$ :

$$\begin{aligned} F_s^S(y) &= \hat{F}_s^S(\theta(y))/A \\ &= -\cos\left(\frac{\pi}{60}\theta(y)\right) + 2.4 \exp\left[-\left(\frac{\theta(y)}{12}\right)^2\right] \\ &\quad - 0.6, \end{aligned} \quad (9)$$

where the mapping  $\theta(y)$  is again given by [Eq. \(5\)](#). The function  $F_s^S(y)$  is plotted in [Fig. 2](#) (dashed line). The freshwater flux is equivalent to a (virtual) diffusive salt flux with

$$\begin{aligned} \frac{\partial S}{\partial z} &= -\frac{\lambda H S_s}{\kappa_v \Delta S} \hat{F}_s^S(\theta) = -\frac{\lambda H S_s A}{\kappa_v \Delta S} F_s^S(y) \\ &= -\sigma_s F_s^S(y). \end{aligned} \quad (10)$$

Here  $S_s$  is a characteristic salinity for the ocean surface, taken to be 36.0 psu. Using the parameter values from [Table 1](#), we obtain a dimensionless amplitude  $\sigma_s = 9.5$  for the surface salt flux.

## 2) LATERAL FLUXES

The Atlantic thermohaline circulation does not consist of the NADW overturning cell alone. It is a complex combination of two overturning cells, with deep water also forming in the Antarctic region. The part of this AABW that flows into the Atlantic Ocean is converted into a brand of deep water called Lower NADW (LNADW): It is exported from the Atlantic again just above the level at which it entered ([Schmitz 1995](#)). [Stocker et al. \(1992\)](#) have shown that these overturning cells interact and that the strength of the NADW cell is influenced by the strength of the AABW circulation. In our study we are principally interested in the interplay between surface processes and interbasin fluxes, and their effect on the deep water formation in the northern part of the Atlantic Ocean. With that objective we designed the Atlantic model configuration [ $q = A$  in [Eq. \(5\)](#)]. This configuration excludes the formation area of AABW, and it is therefore unable to model the dynamics of the bottom water circulation and its interaction with the NADW cell. To make the lateral forcing in our model consistent with this exclusion, we eliminate the influence of AABW by truncating our heat and salt flux profiles ([Fig. 1](#)) at the depth below which only AABW and LNADW are assumed to be present. This depth was found by integrating the meridional mass transport across  $30^\circ\text{S}$  downward. It reversed sign at depth  $H_N = 2828 \text{ m}$ , and we assume that all NADW export above this

depth is compensated by the import of shallower water masses.

The total heat and salt flux profiles  $\hat{F}_l^T(z^*)$  and  $\hat{F}_l^S(z^*)$  of [Figs. 1](#) are approximated by functions of the form  $B[\exp(z^*/a) - b \cos(2\pi z^*/c)]$ , yielding the dimensionless flux profiles  $F_l^T(z)$  and  $F_l^S(z)$  ([Fig. 4](#)):

$$\hat{F}_l^T(z^*(z))/B^T \approx \exp[21(z-1)] - 0.04 \cos[4(z-1)] = F_l^T(z) \quad (11a)$$

and

$$\hat{F}_l^S(z^*(z))/B^S \approx -\exp[8(z-1)] - 0.08 \cos[4(z-1)] = F_l^S(z), \quad (11b)$$

where  $z^* = H_N(z-1)$  and  $H_N = 2828$  m are used. The amplitudes  $B^T$  and  $B^S$  are  $0.30 \text{ MW m}^{-2}$  and  $4.13 \text{ g m}^{-2} \text{ s}^{-1}$ . The advective heat flux is equivalent to a prescribed diffusive flux with

$$\begin{aligned} \frac{\partial T}{\partial y} &= -\frac{L}{\kappa_h \Delta T \rho_0 c_p} \hat{F}_l^T(z^*) = -\frac{H^2 B^T}{\kappa_v L \Delta T \rho_0 c_p} F_l^T(z) \\ &= -\tau_l F_l^T(z). \end{aligned} \quad (12)$$

Assuming a  $\Delta T$  of  $25^\circ\text{C}$ , the parameter  $\tau_l$  takes the value 75.0. Accordingly, the advective salt flux is equivalent to a prescribed diffusive flux when

$$\begin{aligned} \frac{\partial S}{\partial y} &= -\frac{\lambda L}{\kappa_h \Delta S \rho_0} \hat{F}_l^S(z^*) = -\frac{\lambda H^2 B^S}{\kappa_v L \Delta S \rho_0} F_l^S(z) \\ &= -\sigma_l F_l^S(z). \end{aligned} \quad (13)$$

Using the parameter values of [Table 1](#), we obtain a dimensionless amplitude  $\sigma_l$  of 16.5. Note that the amplitude of the lateral heat flux is almost 5 times as large as the lateral salt flux, and 7.5 times as large as the surface salt flux.

In this study we will focus on steady-state solutions, so the balances of heat and salt must be closed. Since in our model the salt flux is prescribed at all boundaries and is taken zero at the bottom and the northern boundary, we have to take care that the net surface salt flux equals the net lateral salt flux. It is therefore convenient to split the surface salt flux  $F_s^S(y)$  and the lateral salt flux  $F_l^S(z)$  into the net components,  $I_s^S$  and  $I_l^S$ , and the shapes,  $\tilde{F}_s^S(y)$  and  $\tilde{F}_l^S(z)$ , which have zero integral. In most cases we will use  $\sigma_s \tilde{F}_s^S(y) + \sigma_l I_l^S$  as surface salt flux rather than  $F_s^S(y)$  to assure that the net lateral salt flux is balanced by a net surface salt flux of equal magnitude. With  $I_l^S < 0$ , this extra surface salt input corresponds to net evaporation from the basin.

The stationary form of Eqs. (6) and the boundary conditions of Eqs. (7) are discretized on a nonequidistant grid: vertically the grid refines upward, while horizontally the grid refines in both directions. Most computations were performed on a grid with 121 grid points in the meridional direction, and 61 in the vertical direction. A steady-state solver is used to obtain stationary solutions. Branches of these steady states are followed through parameter space using a branch-following technique as described in [Dijkstra et al. \(1995\)](#).

#### d. Integral characteristics

In this study we want to examine and understand the response of the overturning strength to changes in the thermohaline forcing. We will analyze the behavior of the solutions by investigating integral balances of the system. This approach has the advantage that nonlinear advective terms are eliminated, and that only volume-integrated and boundary properties are relevant.

#### 1) ENERGY BALANCE



Denoting volume integration by angle brackets, the volume-integrated potential energy  $U$  is defined as  $U = -\langle zB \rangle = -\langle z(T - S) \rangle$ , where  $B = T - S$  is the buoyancy (note that the buoyancy ratio  $\lambda$  has been absorbed in  $S$ ). Multiplying the advection–diffusion equation of buoyancy by  $z$  and integrating over the model domain, we obtain

$$\frac{dU}{dt} = \Delta B_v + \oint z \mathbf{F} \cdot \mathbf{n} d\Gamma - \langle wB \rangle, \quad (14)$$

where  $\mathbf{F} (= \mathbf{F}^T - \mathbf{F}^S)$  denotes the boundary fluxes of buoyancy. Here  $\Delta B_v (= \Delta T_v - \Delta S_v)$  is defined as

$$\Delta B_v \equiv \int_0^1 B|_{z=0}^{z=1} dy \quad (15)$$

and represents the (internal) source of potential energy due to (downward) turbulent mixing of buoyancy. In the ocean this mixing is supported by external mechanical energy sources like internal wave breaking, tidal dissipation, and wind stirring (Huang 1998). The second (external) source (or sink) of potential energy in Eq. (14) is brought about by boundary fluxes of potential energy like air–sea buoyancy fluxes or advective exchange with other oceans. The buoyancy production  $\langle wB \rangle (= \langle wT \rangle - \langle wS \rangle)$  indicates potential energy loss due to vertical advection of buoyancy and realizes the conversion of potential energy into kinetic energy.

The balance of kinetic energy is obtained by multiplying the vorticity equation by  $\psi$  and integrating over the domain:

$$\text{Pr}^{-1} \frac{dE}{dt} = \text{Ra} \langle wB \rangle - D. \quad (16)$$

The volume-integrated kinetic energy  $E$  and dissipation  $D$  (note that  $D \geq 0$ ) are given by

$$E = \frac{1}{2} \langle \psi_z^2 + a^2 \psi_y^2 \rangle \quad (17a)$$

$$D = -\langle \psi \nabla^2 \Omega \rangle = \langle \psi_{zz}^2 + (1 + a^2) \psi_{yz}^2 + a^2 \psi_{yy}^2 \rangle. \quad (17b)$$

In a steady state the time derivatives in Eqs. (14) and (16) are zero, so the right-hand sides of the equations must vanish. Consequently, the buoyancy production  $\langle wB \rangle$  simply relates the (internal and external) sources (and sinks) of potential energy to the dissipation of kinetic energy:

$$\langle wB \rangle = \Delta B_v + \oint z \mathbf{F} \cdot \mathbf{n} d\Gamma \quad (18a)$$

$$\text{Ra} \langle wB \rangle = D. \quad (18b)$$

In our study we combine a buoyancy flux  $F_s(y)$  at the surface with a flux  $F_l(z)$  at the southern boundary of our domain. These fluxes can be split into a net component  $I_s$  and  $I_l$ , which are equal in a steady state, and shape functions  $\tilde{F}_s(y)$  and  $\tilde{F}_l(z)$ , which have zero integral. For this configuration the boundary integral in Eq. (18a) is evaluated in appendix B, and equals

$$\oint z \mathbf{F} \cdot \mathbf{n} d\Gamma = \frac{1}{2} I_s - K_v, \quad (19)$$

where  $K_v (= K_v^T - K_v^S)$  is defined as

$$K_v \equiv \int_0^1 z \tilde{F}_l(z) dz \quad (20)$$

and contains information on the shape of the lateral buoyancy flux. Note that the boundary integral in [Eq. \(19\)](#) contains no information on the shape of the surface buoyancy flux  $\bar{F}_s$ .

## 2) VORTICITY BALANCE

Analogous to the potential energy, the buoyancy torque  $P$  is defined as  $P = -\langle yB \rangle = -\langle y(T - S) \rangle$ , and a balance similar to [Eq. \(14\)](#) is obtained:

$$\frac{dP}{dt} = \Delta B_h + \oint y \mathbf{F} \cdot \mathbf{n} d\Gamma - \langle vB \rangle. \quad (21)$$

The meridional buoyancy difference  $\Delta B_h (= \Delta T_h - \Delta S_h)$  is defined analogously to  $\Delta B_v$ :

$$\Delta B_h \equiv \int_0^1 B|_{y=0}^{y=1} dz. \quad (22)$$

[Equation \(21\)](#) shows that the buoyancy torque can change due to meridional diffusion of buoyancy, boundary fluxes of buoyancy torque, and meridional advection of buoyancy. Volume integration of the vorticity equation yields the relation

$$\text{Pr}^{-1} \frac{d\langle \Omega \rangle}{dt} = \text{Ra} \Delta B_h + \langle \nabla^2 \Omega \rangle, \quad (23)$$

stating that basin-integrated vorticity can be generated by a meridional buoyancy difference  $\Delta B_h$  and dissipated by viscous friction. In steady state, there is a balance between production and dissipation of buoyancy torque, and of vorticity, via  $\Delta B_h$ :

$$\Delta B_h = \langle vB \rangle - \oint y \mathbf{F} \cdot \mathbf{n} d\Gamma \quad (24a)$$

$$\text{Ra} \Delta B_h = -\langle \nabla^2 \Omega \rangle. \quad (24b)$$

The boundary integral in [Eq. \(24a\)](#) can be analyzed in a similar way as the integral in [Eq. \(18a\)](#). With the same considerations concerning the background potential energy, as outlined in appendix B, applied to the background buoyancy torque, this results in

$$\oint y \mathbf{F} \cdot \mathbf{n} d\Gamma = K_h + \frac{1}{2} I_l, \quad (25)$$

where  $K_h (= K_h^T - K_h^S)$  is defined as

$$K_h \equiv \int_0^1 y \bar{F}_s(y) dy. \quad (26)$$

The boundary integral in [Eq. \(25\)](#) contains information on the shape of the surface buoyancy flux only, but not on the shape of the lateral flux.

## 3) RELATIONS BETWEEN THERMOHALINE CHARACTERISTICS AND $\psi_{\text{MAX}}$

In the former sections we have obtained two balances that relate large-scale properties of the thermohaline distributions to the velocity field. The steady-state kinetic energy balance [Eq. \(18b\)](#) relates the dissipation  $D$  [[Eq. \(17b\)](#)] to the buoyancy production  $\langle vB \rangle$ , and via the potential energy equation [Eq. \(18a\)](#) to boundary values and fluxes of  $T$  and  $S$ . In the limit of small aspect ratio ( $a \rightarrow 0$ ), [Eq. \(17b\)](#) yields a relatively simple relation between  $D$  and  $\psi_{\text{max}}$ , as only two terms in  $D$  remain,

$\langle \psi_{zz}^2 \rangle$  and  $\langle \psi_{yz}^2 \rangle$ , or equivalently  $\langle \mathbf{v}_z^2 \rangle$  and  $\langle \mathbf{v}_y^2 \rangle$ . When considering a solution with one circulation cell, both derivatives are roughly proportional to  $\psi_{\max}$ , as can be shown by a simple estimate of these derivatives (Dijkstra and Molemaker 1997). This yields a relation between  $D$ , and thereby  $\langle wB \rangle$ , and  $\psi_{\max}$ , which is approximately quadratic.

The vorticity balance (24b) relates the meridional buoyancy difference to the vorticity dissipation. This dissipation is linearly related to  $\Omega$ , which in turn is linear in  $\psi$ . This suggests that the relation between  $\Delta B_h$  (or equivalently the meridional large-scale pressure difference) and  $\psi_{\max}$  might also be linear.

#### 4. Impact of lateral fluxes on the overturning strength

##### a. Symmetric versus nonsymmetric basin: Comparison of two NPP states



Since we will study the Atlantic overturning circulation in a domain that is closed at 30°S [ $q = A$  in Eq. (5)], it is important to investigate whether the overturning circulation in such an asymmetric domain is representative for a similar circulation in a domain extending all the way south to 60°S [ $q = G$  in Eq. (5)]. In this section we will show that both models are able to produce a circulation pattern that resembles the zonally averaged overturning circulation in the Atlantic: this circulation is characterized by strong downwelling in the northern part of the basin and weak upwelling in the rest of the basin. In accordance with the nomenclature of Thual and McWilliams (1992), these northern downwelling pole-to-pole states are denoted by NPP.

In order to obtain an Atlantic domain NPP (ANPP) state, an NPP solution was calculated on the global domain (GNPP) first [defined by the mapping  $q = G$  in Eq. (5)]. At  $y = 0.25$  (30°S) the advective and diffusive fluxes of heat and salt were diagnosed, and they were prescribed as diffusive fluxes at  $y = 0$  (30°S) of the Atlantic domain [defined by the mapping  $q = A$  in Eq. (5)]:

$$F_l^T(z) = v(T - T_0) - T_y \quad (27a)$$

$$F_l^S(z) = v(S - S_0) - S_y. \quad (27b)$$

In appendix A it is shown that reference values  $T_0$  and  $S_0$  should be taken equal to the average values of  $T$  and  $S$  in the  $y \geq 0.25$  part of the global domain in order to make the potential energy input of the fluxes equal in both models. The advective part of the fluxes in Eqs. (27) turned out to be about 6 to 9 times smaller than the diffusive parts, so the thermal and saline gradients at 30°S do not differ much between the models.

The streamline patterns of the GNPP state north of 30°S (Fig. 5a ) and the ANPP state (Fig. 5b ) show strong resemblance between the two main NPP circulation cells, which have their cores at the same latitudes and depths. The circulation of the ANPP state is slightly stronger ( $\psi_{\max} = 7.31$ ) than that of the GNPP state ( $\psi_{\max} = 6.01$ ). The Atlantic state shows a well-developed counterrotating circulation cell at the southern boundary, a feature that is much weaker and shallower in the global domain. The thermal and saline fields of the two solutions show strong resemblance as well (not shown). The ANPP state appears to be slightly warmer and saltier at the southern boundary due to downward heat and salt advection by the stronger secondary cell.

Due to the procedure of diagnosing and prescribing the fluxes at 30°S, the ANPP state experiences the same thermohaline coupling with the (virtual) region south of 30°S as the GNPP state north of  $y = 0.25$ . The two models differ primarily in the momentum balances, as in the Atlantic model no exchange of vorticity and kinetic energy with the Southern Ocean is possible. In order to estimate the consequence of this neglect, we calculated the balance of production and dissipation of kinetic energy in the two subdomains of the GNPP state ( $y < 0.25$  and  $y > 0.25$ ). It turns out that only 1.4% of the kinetic energy that has been generated in the northern part is transported to the southern part. This means that the energy balance of the northern subdomain is as good as closed, and that the southern part plays a negligible role in the generation and dissipation of kinetic energy of the large-scale overturning circulation. Later we will show that the balance between production ( $Ra \langle wB \rangle$ ) and dissipation ( $D$ ) of kinetic energy [Eq. (18b)] yields an unequivocal relation between the overturning strength  $\psi_{\max}$  and the large-scale characteristics of the thermohaline fields that determine  $\langle wB \rangle$  [Eq. (18a)]. This suggests that the relation between  $\psi_{\max}$  and  $\langle wB \rangle$  in this northern subdomain of the GNPP state may be quite similar to this same relation in the ANPP state. It therefore seems reasonable to assume that the response of the Atlantic state to changing the lateral heat and salt fluxes will be at least qualitatively similar to the response that the global state would display, were we able to force the same heat and salt fluxes at its interior  $y = 0.25$  position. In the following analyses we assume that the representation of the GNPP state by its cutoff Atlantic counterpart is useful, and we will focus our attention on the NPP

states of the model in the Atlantic configuration.

## b. Realistic lateral fluxes

### 1) LATERAL HEAT FLUX

In this section we investigate the impact of the thermal component of interbasin exchange on the overturning circulation by applying a lateral heat flux  $F_l^T(z)$  [Eq. (11a), solid line in Fig. 4 (b)], which accounts for heat input at a shallow level. Starting from the Atlantic NPP state with  $\sigma_s = 10$  ( $\sigma_l = 0$ ), we increase the heat flux amplitude  $\tau_l$  from 0 to a value of 70, which is a realistic value according to the scaling in Eq. (12).

The strength of the overturning cell, given by the maximum value of the streamfunction  $\psi_{\max}$ , increases significantly as the amplitude  $\tau_l$  of the lateral heat flux is increased (Fig. 6a (b)). The governing terms in the energy balance of Eq. (18a) (Fig. 6b (b)) show that this increase in  $\psi_{\max}$  corresponds to a strong increase in buoyancy production  $\langle wB \rangle$ , reflecting the balance between production and dissipation of kinetic energy [Eq. (18b)]. This increase in  $\langle wB \rangle$  is almost completely accounted for by its thermal component  $\langle wT \rangle$ , as its saline component  $-\langle wS \rangle$  is not affected by the strong increase in overturning strength. This is surprising, as a change in the balance between vertical advection ( $\langle wS \rangle$ ) and diffusion ( $\Delta S_{\mathbf{v}}$ ) of salt was certainly expected in response to a strong increase in basinwide upwelling.

Figure 6b (b) furthermore shows the dominant role played by the boundary integral  $\int z \mathbf{F}^T \cdot \mathbf{n} d\Gamma$ , which, according to Eq. (19), can be split into a contribution from the net flux  $I^T/2$ , and a shape contribution  $-K^T_{\mathbf{v}}$ . It turns out that an increase in net surface cooling tends to strengthen the circulation: buoyancy removal at the surface is a source of potential energy and its contribution to the buoyancy production is positive ( $I^T/2 = 0.027\tau_l$ ). The particular shape of the lateral heat flux counteracts this tendency: its contribution to the buoyancy production is negative ( $-K^T_{\mathbf{v}} = -0.014\tau_l$ ), as heat input at a shallow level stabilizes the stratification and extracts potential energy from the system. However, this weakening effect is too small to balance the strengthening influence of net surface cooling: the sum of both contributions is positive ( $0.013\tau_l$ ) and is responsible for the increase in overturning strength with increasing  $\tau_l$ .

Despite the tendency of the lateral heat flux to stabilize the stratification, the vertical thermal difference  $\Delta T_{\mathbf{v}}$  can be seen to decrease slightly. This reflects an increase in bottom temperature because surface temperatures are fixed. This warming of the deeper part of the basin is related to the increase in circulation strength causing increased northward advection of warm subsurface waters and consequently downwelling of warmer waters.



### 2) LATERAL SALT FLUX

To explore how the saline component of ocean interbasin exchange modifies the overturning circulation, we now add a lateral salt flux to the lateral heat flux of the former section ( $\tau_l = 70$ ). The profile of this salt flux  $F_l^S$  [Eq. (11b), long-dashed line in Fig. 4 (b)] accounts for lateral salt export from the upper layer. The amplitude  $\sigma_l$  is increased from zero to 16, which is a realistic value according to the scaling of Eq. (13). As mentioned before, the  $\sigma_l I^S_l$  net salt export brought about by the lateral salt flux is compensated by salt import through the surface of the same magnitude to maintain a flux balance. This extra surface salt input corresponds to net evaporation from the basin.

The overturning strength increases slightly when  $\sigma_l$  is increased (Fig. 7a (b), solid line). The most relevant terms in the buoyancy production (Fig. 7b (b)) show that this increase is related to a decrease in the positive (weakening) value of  $\langle wS \rangle$  (note that  $B \propto -S$ ). Again the contribution of the boundary fluxes dominate the balance. The net surface salt input removes buoyancy from the surface and increases the buoyancy production by an amount of  $-I^S/2 = 0.055\sigma_l$ . The specific shape of the lateral salt flux exports salt at a shallow level and stabilizes the stratification, thus reducing the buoyancy production by an amount of  $K^S_{\mathbf{v}} = -0.063\sigma_l$ . Contrary to the lateral heat flux, this weakening effect of the lateral salt flux turns out to be large enough to balance, and even exceed, the strengthening effect of net surface salt input.

The stabilizing influence of the shape of the lateral salt flux is also reflected by the decrease and sign reversal of the vertical salinity difference  $\Delta S_{\mathbf{v}}$  in Fig. 7b (b). As  $\Delta S_{\mathbf{v}}$  reflects the basin-integrated diffusive vertical salt flux, this sign


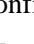

reversal implies that the originally downward diffusive salt flux is reversed, and that salt is now diffused *upward*. This source of potential energy is *indirectly* caused by the shape of the lateral salt flux, and counteracts the weakening *direct* contribution of this shape ( $-K_{\mathcal{V}}^S$ ). The *total* effect of the lateral salt flux is eventually weaker than that caused by the net surface salt input ( $I^S/2$ ), resulting in the slight increase in  $\langle wB \rangle$ .



The suggestion that  $\Delta S_{\mathcal{V}}$  is modified by the particular shape of the lateral salt flux, rather than by a net surface salt flux, is verified in a subsequent case: we increased the amplitude of a *vertically uniform* lateral salt flux  $\sigma_l I_l^S$  ( $I_l^S < 0$ ) from zero to 16. The absence of the vertical profile (Fig. 7a , dashed line) makes the overturning strength much more sensitive to changes in the salt flux strength  $\sigma_l$ ; the relevant terms in the energy balance (Fig. 7c ) show that the strengthening influence of net surface salt input is no longer counteracted by the shape contribution  $-K_{\mathcal{V}}^S$ , as this term is zero in this case. The stratification  $\Delta S_{\mathcal{V}}$  remains unchanged; we can conclude that the vertical profile of the lateral salt flux was largely responsible for changing the stratification in the previous experiment, rather than the net surface salt flux.

### c. Thermohaline forcing and overturning strength



#### 1) LATERAL VERSUS SURFACE FORCING

In this section we examine which changes in the external forcing (the boundary fluxes of buoyancy) tend to affect the overturning strength most. To that end, we compare the sensitivity of the circulation strength to changes in the surface and lateral buoyancy fluxes, and analyze this sensitivity in terms of the two integral balances Eqs. (18) and (24), as introduced in [section 3d](#).

In this section we keep the net flux of salt through the surface and the lateral boundary fixed at  $16I_l^S$  as we independently increase the amplitudes  $\sigma_s$  ( $\sigma_l = 0$ ) and  $\sigma_l$  ( $\sigma_s = 0$ ) of the shapes of the surface and lateral salt fluxes  $\tilde{F}_s^S(y)$  and  $\tilde{F}_l^S(z)$ . The circulation strength  $\psi_{\max}$  turns out to be very sensitive to the amplitude  $\sigma_l$  of the lateral salt flux, whereas the sensitivity to the amplitude  $\sigma_s$  of the surface salt flux is very small (Fig. 8a ). The relevant terms in the buoyancy production confirm that the shape of the lateral flux impacts directly on the balance of potential energy through the term  $-K_{\mathcal{V}}^S$  (Fig. 8b ). The shape of the surface flux, on the other hand, only changes this balance indirectly by modifying the saline stratification  $\Delta S_{\mathcal{V}}$  (Fig. 8c 

The relevant terms in the saline component of  $\Delta B_h$  [Eq. (24a)] show that the change in amplitude  $\sigma_l$  of the lateral salt flux has almost no effect on the balance of the buoyancy torque (Fig. 9a ). The change in the amplitude  $\sigma_s$  of the surface salt flux, however, does influence this balance significantly through the term  $K_h^S$  (Fig. 9b ). This change, reflecting an increase in the meridional transport of freshwater by the atmosphere, is counteracted by an increase in the meridional advection  $\langle \mathcal{U}S \rangle$  rather than by an increase in  $\Delta S_h$ . Increasing the amplitude of the surface salt flux does therefore not result in a significant increase in the vorticity production [Eq. (24b)] or circulation strength.

#### 2) THERMOHALINE FORCING

Equations (18a) and (24a) show that in a steady state changes in the distribution of the boundary fluxes (as reflected by  $K_{\mathcal{V}}$  or  $K_h$ ) must be balanced by changes in advective or diffusive transports. Since our model is in the advective regime, as is the real ocean, changes in  $K_{\mathcal{V}}$  or  $K_h$  appear to be balanced by advection (through  $\langle wB \rangle$  and  $\langle \mathcal{U}B \rangle$ ) rather than by diffusion ( $\Delta B_{\mathcal{V}}$  or  $\Delta B_h$ ) (Figs. 8  and 9 ). This means that changes in the boundary fluxes that impact on the potential energy (e.g., via  $I/2$  or  $K_{\mathcal{V}}$ ) directly influence the conversion of potential to kinetic energy (accomplished by  $\langle wB \rangle$ ), and thereby the flow strength. These changes appear to be really *forced* upon the flow. This does not hold for changes in the boundary fluxes that impact on the buoyancy torque (e.g., via  $K_h$ ). Since these changes are again responded to by advection  $\langle \mathcal{U}B \rangle$  rather than by diffusion  $\Delta B_h$ , they do not directly influence the production of vorticity (accomplished by  $\Delta B_h$ ). In our model the source of vorticity  $\Delta B_h$  is *determined* by the flow rather than that it *forces* the flow.

We conclude that, in our model and in the specific parameter regime studied, the overturning circulation is much more sensitive to variations in the shape and amplitude of the lateral buoyancy fluxes than to similar variations in the surface

fluxes. This is due to the fact that the shapes of the lateral fluxes have a much stronger (direct) impact on the potential energy of the system than those of the surface fluxes, which modify the potential energy only in an indirect way.

## 5. Discussion

### a. Scaling relations

According to the discussion in [section 3d\(3\)](#), we expect the relation between  $\psi_{\max}$  and the buoyancy production  $\langle wB \rangle$  to be approximately quadratic, whereas the relation between  $\psi_{\max}$  and the meridional buoyancy difference  $\Delta B_h$  is expected to be approximately linear. In [Fig. 10](#), the meridional buoyancy difference  $\Delta B_h$  and the buoyancy production  $\langle wB \rangle$  are plotted as a function of  $\psi_{\max}$  for all experiments performed. Linear and quadratic fits to these results are included to indicate that the presumed relations hold quite well in this model.

These two scaling relations displayed by this model correspond to the first-order balances between density gradients and the angular momentum in the meridional plane, which are found in the rotationless limit of a low-order projection of the Navier–Stokes equations ([Van der Schrier and Maas 1998](#)). Their model gives a physical justification to the frequently used box models (e.g., [Stommel 1961](#)), which impose a linear relation between overturning strength and meridional density gradient. However, once rotation is included, this relation is complicated. Scaling relations based on thermal wind balance yield a  $1/3$  power-law relation (e.g., [Bryan 1987](#)) between overturning strength and meridional density scale. Nevertheless, low-resolution OGCMs (e.g., [Rahmstorf 1996](#)) appear to follow the linear relation rather than the power-law dependence when, according to Rahmstorf, most of the NADW upwelling takes place outside the Atlantic.

The quadratic relation between the overturning strength  $\psi_{\max}$  and the buoyancy production  $\langle wB \rangle$  ([Fig. 10](#)) shows that a quadratic relation exists between  $\psi_{\max}$  and a net surface buoyancy flux  $I_s$ , since  $I_s$  contributes directly to  $\langle wB \rangle$  [Eqs. (18) and (19)]. This suggests that the strength of the Atlantic overturning circulation is directly related to the net freshwater export from the Atlantic basin. This is in agreement with the findings of [Zaucker et al. \(1994\)](#) and [Rahmstorf \(1996\)](#), who found a similar relation in different model contexts. In our model this relation is based on the fact that a net surface buoyancy flux is a source of potential energy and that it supplies energy to drive the overturning circulation. We do not know whether the agreement between our model and the models of [Zaucker et al. \(1994\)](#) and [Rahmstorf \(1996\)](#) is based on equivalent physics.

### b. Thermohaline component of the lateral salt flux

In [section 2](#) it was shown that there is a large difference between the total lateral salt flux at 30°S and its overturning component, both in shape and in net transport ([Fig. 1b](#)). As our 2D model lacks the residual transport by the wind-driven gyres, one could argue about which flux to use as appropriate lateral forcing for this model. So far, we have chosen to use the total salt flux, which is the true thermohaline flux, as it is consistent with net evaporation from the Atlantic basin. However, this choice forces the overturning circulation or unrealistically strong meridional diffusion to account for net evaporation, whereas in reality this is accounted for by the wind-driven gyre circulation. The large southward salt flux across 30°S, for instance, is represented in our model by a diffusive flux at the southern boundary. This requires a meridional gradient in salinity that freshens the surface layers, although in reality Atlantic thermocline salinities are extremely high. On the other hand, prescribing the overturning component of the salt flux gives a wrong sign to the net flux. It might, however, give more credit to the thermohaline structure in the Atlantic: the large influx of thermocline water saltens the surface layer, while a fresh subsurface layer might be generated by the salt export at intermediate depths (long-dashed line in [Fig. 1b](#)).

To study the consequence of prescribing the overturning component of the salt flux instead of the total flux, we performed a transformation between the total salt flux, as given by [Eq. \(11b\)](#) and here denoted  $F_{l,\text{total}}$ , and a representation of the overturning component,  $F_{l,\text{overturning}}$ , as follows:

$$F_l(z) = (1 - \mu)F_{l,\text{total}}(z) + \mu F_{l,\text{overturning}}(z). \quad (28)$$

The main characteristics of the overturning salt flux (strong salt input in the upper layer, an export maximum at subsurface levels, and net salt import) are well modeled by a flux of the following form (short-dashed line in [Fig. 4](#)):

$$F_{l,\text{overturning}}(z) = \cos[12.4(z - 1)] \exp[8.0(z - 1)] + 0.05, \quad (29)$$

which was obtained by fitting the function to the upper 2828 m of the overturning salt flux ([Fig. 1b](#)). The

transformation is performed at  $\sigma_s = 10$ ,  $\tau_l = 70$ , and  $\sigma_l = 16$ .

The terms governing the buoyancy production show a significant change as  $\mu$  is changed from 0 ( $F_l^S = F_{l,\text{total}}^S$ ) to 1 ( $F_l^S = F_{l,\text{overturning}}^S$ ) (Fig. 11): the weakening effect of salinity ( $\langle wS \rangle > 0$ ) increases with  $\mu$ , resulting in a decrease in overturning strength from about 10 to 8. It turns out that the net surface flux and the shape of the lateral profile interchange their roles in the energy balance during the transformation: the net surface salt source changes into a salt sink, losing its positive contribution to the buoyancy production ( $-I^S/2 > 0$ ), and ending up weakening the flow ( $-I^S/2 < 0$ ). Accordingly, as the shape changes from a shallow salt sink to a shallow salt source, its originally weakening influence ( $K_{\mathbf{u}}^S < 0$ ) is reversed and becomes a strengthening contribution ( $K_{\mathbf{u}}^S > 0$ ). The difference between the total salt flux profile and its overturning component is confined to the upper 20% of the domain. This leaves the vertical displacement of salt from its source to its sink relatively small: the buoyancy generated by advecting salt from the surface to the shallow lateral salt sink ( $\mu = 0$ , total lateral salt flux) is small, as is the buoyancy that is lost by uplifting salt from its lateral source to the surface ( $\mu = 1$ , overturning component). In fact, it is this change in direction that causes the increase in  $I^S/2 - K_{\mathbf{u}}^S$ . Figure 11 also shows a rather strong increase in the saline stratification. This clearly shows the ability of the overturning salt flux to increase the salinities of the surface waters.

We have seen that the two-dimensionality of our model, and consequently the lack of the essentially horizontal gyre transport, makes a consistent representation of the salt transports and forcing very difficult. The transformation experiment has illustrated the differences between two possible flux profiles: although prescribing the total salt flux is the most consistent choice with respect to the sign of the net salt flux, the overturning component is more consistent with [Rahmstorf's \(1996\)](#) concept of active freshwater forcing. However, we do not know the surface profile of this active freshwater forcing, and just adding a constant freshwater input to the observed profiles of  $E - P$ , as was done in this study, is also quite arbitrary. These results indicate that care should be taken when using 2D models, as they fail to resolve residual fluxes of heat and salt properly.

### c. The model


#### 1) THE ENERGY BALANCE

Although the model is not appropriate to quantify the processes studied, we believe that it has shown basic principles governing the operation of the overturning circulation that may be independent of details of the model: when the basin-integrated energy balances of the real ocean or of a realistic ocean model are calculated, then these integral balances are governed by very much the same processes as described in this paper. The only relevant mechanism of potential energy removal not represented in this model is mesoscale convection. [Bryan \(1987\)](#) and [Huang \(1998\)](#) analyzed the energy cycles of a single-hemispheric GCM with rectangular geometry, driven by thermohaline forcing and with (Bryan) and without (Huang) wind forcing. In both studies mesoscale convection turned out to be the largest sink of potential energy, and only a small fraction (generally some 10%) of the energy input by vertical mixing (equivalent to  $\Delta B_{\mathbf{u}}$  in our model) was directly converted into kinetic energy of the large-scale overturning circulation.

In general, the potential energy  $U$  of a density-driven fluid in motion contains a background component  $U_r$  and a component known as available potential energy  $U_a$ , which is the amount of energy that would be released if the flow were halted and the density field settled in its least energetic distribution, with energy content  $U_r$  ([Huang 1998](#)). Contrary to the potential energy  $U$ , for instance, the available potential energy  $U_a$  can be modified by the meridional distribution of surface buoyancy fluxes, albeit at the expense of  $U_r$ . For a transient system, the time evolution of the available potential energy  $U_a$  might give a better description of the behavior of the system since the reference energy  $U_r$  can be considered as merely “dead weight,” and is not available to drive the flow. To that end it is comparable to the basin-averaged potential energy  $U_0$ , as introduced in appendix B of this paper. In this study, however, we only considered steady-state solutions. For these states the sources and sinks of  $U$  and of  $U_a$  are ultimately the same since the reference energy  $U_r$  (as well as  $U$  and  $U_a$ ) is constant. Furthermore, as we focused on energy conversions, the exact values of the energies  $U$ ,  $U_a$ , and  $U_r$  were not relevant. Although the  $U_a$  contents of a solution is the amount of potential energy that *could be* converted into kinetic energy, we studied the amount of energy that *was* converted into kinetic energy.

#### 2) THE 30°S BOUNDARY

The presence of the boundary at 30°S results, of course, in a rather poor representation of the overturning circulation

since in reality most of the NADW leaves the Atlantic to spread out over the entire World Ocean instead of being upwelled north of 30°S. Due to this NADW export and the corresponding return transports, the Atlantic exchanges momentum with the Southern Ocean, leaving the balances of kinetic energy and vorticity in the Atlantic Ocean open. The magnitude of this exchange in the real ocean and its importance for the overall balances is not known. Therefore, we cannot assess how the neglect of this exchange modifies the sensitivity of the circulation strength to changes in the thermohaline forcing. In [section 4a](#) we have shown that there is a strong similarity between the Atlantic NPP state and the global domain NPP state, which is similar to the NPP states found in equivalent models of the thermohaline overturning circulation (e.g., [Quon and Ghil 1992, 1995](#); [Dijkstra and Molemaker 1997](#)). However, since most of the upwelling in the global domain takes place north of 30°S as well ([Fig. 5a](#) ) , this state is not representative for the multibasin thermohaline circulation.

Although in our model the exchange of kinetic energy with the southern part of the Atlantic is neglected, the exchange of potential energy is captured correctly by our approach of prescribing the lateral fluxes of heat and salt. The *nature* of buoyancy fluxes, whether advective or diffusive, is not relevant for the basin-integrated balance of potential energy in the Atlantic [[Eq. \(18a\)](#)].

In our model we have shown that the overturning circulation exhibits a strong sensitivity to a net surface buoyancy flux, for instance, due to net surface cooling or net evaporation. In reality, however, the thermohaline overturning circulation is a global circulation pattern, with upwelling in the ACC, and in the Pacific and Indian Oceans. The heat or freshwater that is extracted from the Atlantic must be compensated by heat and freshwater input in the other basins. This buoyancy input on the upwelling branch of the overturning circulation would undo the potential energy gain of the Atlantic. The fact that the quadratic relation between the overturning strength and net Atlantic evaporation is found in models that do include the Pacific (cf. [section 5a](#)) might give rise to the speculation that the energy gain of the Atlantic is not completely undone in the rest of the World Ocean. Indeed, there is evidence that a part of the NADW upwelling is accomplished in the wind-driven upwelling regimes of the ACC rather than by slow uniformly distributed and buoyancy driven upwelling ([Toggweiler and Samuels 1993b](#); [Shriver and Hurlburt 1997](#); [Döös and Coward 1997](#)). This implies that the wind-driven upwelling might supply at least a part of the energy needed for driving the Atlantic overturning circulation.

As advective fluxes are directly linked to the circulation, it is probable that feedback effects exist between the overturning strength and the lateral fluxes that could not be captured by our model. It is not clear how the advective heat and salt fluxes would respond to a change in the overturning circulation, as such a change will not only modify the flow field but also the distributions of heat and salt. It is therefore not possible to anticipate whether these feedbacks increase or decrease the sensitivity of the flow strength to changes in the lateral fluxes.

### 3) SURFACE BOUNDARY CONDITIONS

There are numerous feedbacks between the ocean and the atmosphere that can seriously affect the sensitivity and stability of the ocean's overturning circulation ([Rahmstorf et al. 1996](#)), and it is therefore important to take these into account in climate sensitivity studies. In this study we have forced the circulation at the surface with mixed boundary conditions for temperature and salinity, which are among the simplest representations of ocean–atmosphere interaction possible. Although this choice might not be realistic, it is certainly illustrative for the fact that the equilibration timescale of a sea surface temperature anomaly is much smaller (here taken to be zero) than that of a sea surface salinity anomaly (here taken to be infinity).

It was shown that in this model the overturning circulation is relatively insensitive to changes in the meridional distribution of the surface buoyancy flux, as this distribution does not impact on the potential energy balance. Unless the *net* surface buoyancy flux is modified, the influence of more realistic surface boundary conditions on the energy balance will be confined to changes in the vertical buoyancy difference  $\Delta B_{\nu}$ . However, the fact that in our model  $\Delta T_{\nu}$  was partially constrained by the fixed surface temperatures, whereas  $\Delta S_{\nu}$  was unconstrained, did not result in large differences in the response to changing thermal and saline forcing. Therefore we do not expect a large change in the role of  $\Delta B_{\nu}$  when more active boundary conditions are applied. It is therefore improbable that incorporation of more active air–sea interaction will drastically change the sensitivity of the circulation to changing forcing. However, for the time-dependent response of the system the choice of boundary conditions may be essential.

#### *d. Implications for the impact of Agulhas leakage*

What can we say about the importance of Agulhas leakage for the conveyor belt circulation? Does the Indian–Atlantic interbasin exchange of heat and salt through the Agulhas leakage significantly influence the overturning strength, as was speculated earlier ([Gordon 1986](#); [Gordon et al. 1992](#))? What will happen if Agulhas leakage is shut off and the South Atlantic surface salinities drop by about 0.5 psu?

A decrease in South Atlantic surface salinities will probably not influence the *net* flux of salt across 30°S dramatically.



Retrieving a certain amount of freshwater ( $E - P$ ) from slightly fresher surface water will reduce the virtual salt flux, and consequently the surface buoyancy removal. On the other hand, reduction of the section-averaged salinity at 30°S reduces the salt flux brought about by the net mass transport across that section (Bering Strait transport minus the amount of  $E - P$ ). This reduction has to be compensated by salt fluxes induced by the overturning or the gyre circulations. These changes, however, will influence the net flux of salt by less than 1.5% and, as they work in the opposite direction, might cancel each other out.

The influence of reduced Agulhas leakage on the *shape* of the salt flux profile may be more important, as a 0.5 psu drop in a 2.0 psu salinity *anomaly* is significant. According to Eq. (4), it is the overturning component of the salt flux that is directly related to the mean surface salinity anomaly (referred to the Atlantic mean salinity  $S_0$ ) of the South Atlantic, and internal processes will determine whether the circulation responds to a decreased salt flux by changing the residual component of the salt flux (involving the zonal salinity structure of the South Atlantic thermocline), or by changing the overturning component (involving the salt stratification of the whole Atlantic, or the overturning circulation itself). A change in the latter will influence the circulation strength most, as it involves vertical advective fluxes of buoyancy by the meridional overturning circulation.

Freshening of Atlantic surface waters might reduce the convective activity in the formation region of NADW, as suggested by [Gordon et al. \(1992\)](#), and so reduce the production of deep water. On the other hand, the resulting reduction of the salinity stratification will enhance the downward diffusion of buoyancy, which turned out to be a (relatively small) source of potential energy in our model.

What about heat input by Agulhas leakage? If Agulhas leakage can be held partly responsible for the large northward heat flux in the South Atlantic ([Thompson et al. 1997](#)), it is also responsible for large atmospheric heat loss in the Atlantic. When the influence of this northward heat flux on evaporation is considered ([Gordon 1986](#)), then Agulhas heat input might be responsible not only for net surface cooling, but also for net surface saltening. As in our model surface buoyancy loss turned out to be the largest source of potential energy, shutting off the Agulhas leakage might have a double impact on the energy balance of the Atlantic, and result in a reduction in the overturning strength. An interesting possibility is therefore that not the Agulhas salt input but the Agulhas heat input influences the overturning strength most.

Can we now explain the results obtained by [Cai and Greatbatch \(1995\)](#)? In their model, shutting off Agulhas leakage did not influence the outflow rate of deep water. They argued that the thermal and saline changes canceled each other out, leaving the density field almost unaffected. Nevertheless, several aspects of the thermohaline circulation seemed to have changed as a response to shutting off Agulhas leakage, and some of these changes might have had some influence on the balance of potential energy in the model ocean: the net northward heat flux across 30°S seemed to have been reduced (their Fig. 12), and consequently the surface buoyancy loss and the associated potential energy gain; there appeared to have been a warming and saltening of the surface waters in the northern North Atlantic, possibly due to reduction of the deep convection in this region, which would have caused a reduction in the associated sink of potential energy; although the thermal and saline changes might have canceled, the shift of 0.7 Sv ( $\text{Sv} \equiv 10^6 \text{ m}^2 \text{ s}^{-1}$ ) from thermocline to intermediate water masses might have changed the shape contribution of the lateral buoyancy flux. It is therefore not clear whether in the model of [Cai and Greatbatch \(1995\)](#) none of these changes in the potential energy balance was large enough to influence the overturning strength or if several effects canceled, leaving the NADW outflow unchanged.

The results of this study have shown that the overturning strength is very sensitive to details of the interbasin fluxes of heat and salt. This means that an impact of the Agulhas leakage on the overturning circulation is probable. At the same time, it emphasizes the possible importance of the south Indian Ocean wind regimes for the thermohaline circulation, as this seems to be controlling the amount of Agulhas leakage. Influence of Southern Hemisphere winds on Atlantic overturning strength has been suggested previously by [Toggweiler and Samuels \(1993a\)](#), although they propose a different mechanism: they argue that the deep southward transport below the Drake Passage sill depth, required to compensate for unbalanced northward Ekman transport in the Drake Passage latitude band, can be derived only from North Atlantic downwelling. In their numerical experiments the Atlantic overturning strength is governed by this Ekman inflow rather than by thermohaline forcing. [Rahmstorf and England \(1997\)](#), however, have shown that the use of the mixed boundary conditions by [Toggweiler and Samuels \(1993a\)](#) suppresses the role of the thermohaline component of the overturning circulation. Using more realistic boundary conditions, they show that the contribution of Drake Passage Ekman flows is only a fraction of the total amount of NADW formed.

## 6. Summary and conclusions

In the first part of this paper we analyzed the thermohaline exchange between the Atlantic Ocean north of 30°S and the Southern Ocean. We used an inversion of hydrographic data, including recent WOCE data, to calculate the meridional heat and salt fluxes across the Atlantic 30°S section. A large difference between the total lateral salt flux and its overturning component turned out to be the most striking feature of the zonally averaged profiles. As the former yielded a net southward salt flux, consistent with net Atlantic evaporation, the latter was characterized by a northward net flux, indicating that on

average the exported NADW is fresher than the compensating return flows. This confirms the idea of [Rahmstorf \(1996\)](#) that salt transports due to the horizontal, wind-driven, gyre circulation are an essential component of the Atlantic salt budget.

We studied the influence of these lateral fluxes on the strength and operation of the overturning circulation by prescribing them at the southern boundary of a simple two-dimensional model of the Atlantic Ocean. The sensitivity of the flow strength to changes in this lateral forcing was examined and analyzed in terms of integral balances of the system. The main advantage of this approach is that the results are rather independent of the details of the momentum balance, indicating that the conclusions drawn in this study may be relevant for the real ocean.

The analyses have shown that especially the *net* components of the heat and salt fluxes have a large positive impact on the overturning strength in our model. Both net surface cooling (corresponding to a northward heat flux at 30°S in the Atlantic) and salting (due to excess evaporation in the Atlantic) are sources of potential energy of the system and tend to strengthen the flow. The *shapes* of the lateral flux profiles turn out to have a dual influence on the potential energy of the system. As their particular shapes tend to stabilize the stratification, they extract potential energy from the system directly and tend to weaken the flow. This effect is slightly counteracted by an increase in the downward diffusion of buoyancy, which is a source of potential energy. The results of this study also indicate that, in the parameter regime considered, the circulation strength is more sensitive to changes in the shape of the lateral buoyancy flux than to changes in the meridional distribution of the surface buoyancy flux, as the latter does not explicitly change the potential energy input of the system.

We conclude, on the basis of this study, that not only the amount of heat or salt that is imported into the Atlantic is relevant for the operation of the overturning circulation, but that also the vertical distribution of this exchange is relevant. A climatological shift in the importance of intermediate or thermocline water for compensating NADW export, or a change in the thermohaline characteristics of these water masses, might therefore influence the Atlantic overturning strength considerably.

This study has shown the importance of interocean fluxes of heat and freshwater, caused by the atmosphere and the ocean, for the operation of the global-scale ocean circulation. This emphasizes the need for truly global models for studies of climate dynamics and climate change, and for correct representations of the interbasin fluxes in these models. The model results and the analysis of the hydrographic data also emphasize one of the major shortcomings of 2D models, which fail to account for residual wind-driven fluxes of heat and salt. Care should be taken when using these models for sensitivity studies of the thermohaline circulation, as [Rahmstorf \(1996\)](#) has shown that the sign of the net active freshwater flux is crucial for the stability of overturning states.

### Acknowledgments

We thank Dr. Jürgen Holfort from the Institut für Meereskunde, Kiel, Germany, for making the data of his inversion available to us. We thank two reviewers for their constructive comments. WW, PJJ, and WR were supported by NOP II Grant 013001237.10. The contribution of HD was sponsored by NWO PIONIER Grant 030-76-187. All computations were performed on the CRAY Y-MP C98 at the Academic Computer Centre (SARA) Amsterdam, the Netherlands, within the projects SC-479 and SC-212. Use of these computing facilities was sponsored by the Stichting Nationale Computerfaciliteiten (National Computing Facilities Foundation), with financial support from the Nederlandse Organisatie voor Wetenschappelijk Onderzoek (Netherlands Organization for Scientific Research).

---

### REFERENCES

- Baumgartner, A., and E. Reichel, 1975: *The World Water Balance*. Elsevier, 179 pp..
- Broecker, W. S., 1991: The great ocean conveyor. *Oceanography*, **4**, 79–89..
- , M. Peteet, and D. Rind, 1985: Does the ocean–atmosphere system have more than one stable mode of operation? *Nature*, **315**, 21–26..
- Bryan, F., 1987: Parameter sensitivity of primitive equation ocean general circulation models. *J. Phys. Oceanogr.*, **17**, 970–985.. [Find this article online](#)
- Cai, W., and R. J. Greatbatch, 1995: Compensation for the NADW outflow in a global ocean circulation model. *J. Phys. Oceanogr.*, **25**, 226–241.. [Find this article online](#)
- Cessi, P., and W. R. Young, 1992: Multiple equilibria in two-dimensional thermohaline circulation. *J. Fluid Mech.*, **241**, 291–309..
- Chandrasekhar, S., 1961: *Hydrodynamic and Hydromagnetic Stability*. Clarendon Press, 652 pp..

- De Ruijter, W. P. M., 1982: Asymptotic analysis of the Agulhas and Brazil Current systems. *J. Phys. Oceanogr.*, **12**, 361–373.. [Find this article online](#)
- , A. Biastoch, S. S. Drijfhout, J. R. E. Lutjeharms, R. P. Matano, T. Pichevin, P. J. van Leeuwen, and W. Weijer, 1999: Indian–Atlantic inter-ocean exchange: Dynamics, estimation and impact. *J. Geophys. Res.*, in press..
- Dijkstra, H. A., and M. J. Molemaker, 1997: Symmetry breaking and overturning oscillations in thermohaline driven flows. *J. Fluid Mech.*, **331**, 169–198..
- , — , A. van der Ploeg, and E. F. F. Botta, 1995: An efficient code to compute non-parallel steady flows and their linear stability. *Comput. Fluids*, **24**, 415–434..
- Döös, K., and A. Coward, 1997: The Southern Ocean as the major upwelling zone of North Atlantic Deep Water. *Int. WOCE Newslett.*, **27**, 3–4..
- Drijfhout, S. S., E. Maier-Reimer, and U. Mikolajewicz, 1996: Tracing the conveyor belt in the Hamburg LSG ocean general circulation model. *J. Geophys. Res.*, **101**, 22 563–22 575..
- Gordon, A. L., 1985: Indian–Atlantic transfer of thermocline water at the Agulhas Retroflection. *Science*, **227**, 1030–1033..
- , 1986: Interocean exchange of thermocline water. *J. Geophys. Res.*, **91**, 5037–5046..
- , R. F. Weiss, W. M. Smethie Jr., and M. J. Warner, 1992: Thermocline and intermediate water communication between the South Atlantic and Indian Oceans. *J. Geophys. Res.*, **97**, 7223–7240..
- Holfort, J., 1994: *Großräumige Zirkulation und meridionale Transporte im Südatlantik* (Large-scale circulation and meridional transports in the South Atlantic). Ph.D. dissertation, Institut für Meereskunde Kiel, 96 pp..
- Howard, W. R., and W. L. Prell, 1992: Late quaternary surface circulation of the southern Indian Ocean and its relationship to orbital variations. *Paleoceanography*, **7**, 79–117..
- Huang, R. X., 1998: Mixing and available potential energy in a Boussinesq Ocean. *J. Phys. Oceanogr.*, **28**, 669–678.. [Find this article online](#)
- Keigwin, L. D., G. A. Jones, and S. J. Lehman, 1991: Deglacial meltwater discharge, North Atlantic deep circulation, and abrupt climate change. *J. Geophys. Res.*, **96**, 16 811–16 826..
- Levitus, S., 1982: *Climatological Atlas of the World Ocean*. NOAA Prof. Paper No. 13, U.S. Govt. Printing Office, 173 pp..
- Lutjeharms, J. R. E., 1996: The exchange of water between the South Indian and South Atlantic Oceans. *The South Atlantic: Present and Past Circulation*, G. Wefer et al., Eds., Springer, 125–162..
- McCann, M. P., A. J. Semtner Jr., and R. M. Chervin, 1994: Transports and budgets of volume, heat, and salinity from a global eddy-resolving ocean model. *Climate Dyn.*, **10**, 59–80..
- Oort, A. H., 1983: *Global Atmospheric Circulation Statistics, 1985–1973*. NOAA Prof. Paper No. 14, U.S. Govt. Printing Office, 180 pp..
- Piola, A. R., and A. L. Gordon, 1986: On oceanic heat and freshwater fluxes at 30°S. *J. Phys. Oceanogr.*, **16**, 2184–2190.. [Find this article online](#)
- Quon, C., and M. Ghil, 1992: Multiple equilibria in thermosolutal convection due to salt-flux boundary conditions. *J. Fluid Mech.*, **245**, 449–483..
- , and — , 1995: Multiple equilibria and stable oscillations in thermosolutal convection at small aspect ratio. *J. Fluid Mech.*, **291**, 33–56..
- Rahmstorf, S., 1996: On the freshwater forcing and transport of the Atlantic thermohaline circulation. *Climate Dyn.*, **12**, 799–811..
- , and M. H. England, 1997: Influence of Southern Hemisphere winds on North Atlantic Deep Water flow. *J. Phys. Oceanogr.*, **27**, 2040–2054.. [Find this article online](#)
- , J. Marotzke, and J. Willebrand, 1996: Stability of the thermohaline circulation. *The Warm Water Sphere of the North Atlantic*, W. Krauss, Ed., Bornträger, 129–158..
- Rintoul, S. R., 1991: South Atlantic interbasin exchange. *J. Geophys. Res.*, **96**, 2675–2692..

Shriver, J. F., and H. E. Hurlburt, 1997: The contribution of the global thermohaline circulation to the Pacific to Indian Ocean throughflow via Indonesia. *J. Geophys. Res.*, **102** (C3), 5491–5511..

Stocker, T. F., D. G. Wright, and W. S. Broecker, 1992: The influence of high-latitude surface forcing on the global thermohaline circulation. *Paleoceanography*, **7**, 529–541..

Stommel, H., 1961: Thermohaline convection with two stable regimes of flow. *Tellus*, **13**, 224–230..

—, 1980: Asymmetry of interoceanic fresh-water and heat fluxes. *Proc. Natl. Acad. Sci. USA*, **77**, 2377–2381..

Thompson, S. R., D. P. Stevens, and K. Döös, 1997: The importance of interocean exchange south of Africa in a numerical model. *J. Geophys. Res.*, **102**, 3303–3315..

Thual, O., and J. C. McWilliams, 1992: The catastrophe structure of thermohaline convection in a two-dimensional fluid model and a comparison with low-order box models. *Geophys. Astrophys. Fluid Dyn.*, **64**, 67–95..

Toggweiler, J. R., and B. Samuels, 1993a: Is the magnitude of the deep outflow from the Atlantic Ocean actually governed by Southern Hemisphere winds? *The Global Carbon Cycle*, M. Heidemann, Ed., NATO ASI Series I: Global Environmental Change, Vol. 15, Springer-Verlag, 303–331..

—, and —, 1993b: New radiocarbon constraints on the upwelling of abyssal water to the ocean's surface. *The Global Carbon Cycle*, M. Heidemann, Ed., NATO ASI Series I: Global Environmental Change, Vol. 15, Springer-Verlag, 333–366..

Van der Schrier, G., and L. Maas, 1998: Chaos in a simple model of the three-dimensional, salt-dominated ocean circulation. *Climate Dyn.*, **14**, 489–502..

Wijffels, S. E., R. W. Schmitt, H. L. Bryden, and A. Stigebrandt, 1992: Transport of freshwater by the oceans. *J. Phys. Oceanogr.*, **22**, 155–162.. [Find this article online](#)

Zaucker, F., T. F. Stocker, and W. S. Broecker, 1994: Atmospheric freshwater fluxes and their effect on the global thermohaline circulation. *J. Geophys. Res.*, **99**, 12 443–12 457..

---

## APPENDIX A

### 7. Correct Values for $T_0$ and $S_0$

In this appendix we will show that the appropriate choices for the reference values  $T_0$  and  $S_0$  in Eqs. (4) and Eqs. (27) are the average values of temperature and salinity of the basin under consideration, in this case the Atlantic Ocean north of 30°S. Only then will the potential energy input of these fluxes into the Atlantic be correctly represented in our model.

We consider the evolution-equation for basin-integrated potential energy [Eq. \(14\)](#), the basin under consideration being the Atlantic north of 30°S. No a priori model constraints have been used in deriving this equation: the unspecified boundary buoyancy flux  $\mathbf{F}$  contains the realistic advective flux at the 30°S section or its diffusive model equivalent, so the equation applies both to the Atlantic Ocean and to our model. When we split the vertical velocity  $w$  into the basin-averaged part  $w_0 = \langle w \rangle$  and a deviation  $w'$ , we can write the buoyancy production as

$$\langle wB \rangle = w_0 \langle B \rangle + \langle w'B \rangle. \quad (A1)$$

As the real ocean is not closed at 30°S and mass exchange takes place with the Southern Ocean, the net vertical transport  $w_0$  will not vanish. This means that in reality we have, besides the residual term  $\langle w'B \rangle$ , a change in potential energy due to net vertical flow advecting the average buoyancy  $\langle B \rangle$ . In our model  $w_0$  is zero, as the model domain is closed. In order to make the buoyancy production in our model comparable to that in the real ocean, the term  $w_0 \langle B \rangle$  must vanish. The definition of  $B^* = \rho_0 [\alpha(T^* - T_0) - \beta(S^* - S_0)] = \rho_0 \alpha \Delta T (T - \lambda S) = B_0 B$  now shows that the correct choice for  $T_0$  and  $S_0$  is to take the basin-averaged values: only then do the diffusive fluxes in our 2D model represent the potential energy input of the real advective fluxes in a comparable way.

---

## 8. Potential Energy and the Basin-Integrated Value

The explicit appearance of the vertical coordinate  $z$  in the definition of potential energy, as well as in the boundary integral  $\int z \mathbf{F} \cdot \mathbf{n} d\Gamma$  of Eq. (18), might give rise to some ambiguity about the invariance of the potential energy formulation with respect to the particular choice of the reference level. Obviously a potential energy  $U'(\Delta z) = -\langle (z - \Delta z) B \rangle$ , which is defined with respect to a reference level  $\Delta z$  above the bottom, is  $\Delta z \langle B \rangle$  larger than  $U$ , while the boundary integral  $\int (z - \Delta z) \mathbf{F} \cdot \mathbf{n} d\Gamma$  is an amount  $\Delta z \int \mathbf{F} \cdot \mathbf{n} d\Gamma$  smaller. As the behavior of our system must be independent of the choice of reference level, the time evolutions of  $U$  and  $U'(\Delta z)$  are linked via

$$\frac{d}{dt} \langle B \rangle = - \oint \mathbf{F} \cdot \mathbf{n} d\Gamma = -I, \quad (\text{B1})$$

where  $I$  is the net boundary buoyancy flux (positive outward). In steady-state conditions, both  $d\langle B \rangle/dt$  and  $I$  must evidently be zero. We can split the potential energy  $U$  into a basin-averaged part  $U_0 = -\langle z \rangle \langle B \rangle = -\langle B \rangle/2$  and a deviation  $\tilde{U} = -\langle z(B - \langle B \rangle) \rangle = U + \langle B \rangle/2$ . The time evolution of  $U_0$  equals

$$\frac{dU_0}{dt} = -\frac{1}{2} \frac{d}{dt} \langle B \rangle = \frac{1}{2} I \quad (\text{B2})$$

and indicates that  $I/2$  of the contribution of the boundary fluxes is used for increasing the background state  $U_0$ . A change in this background potential energy, however, is not relevant from a dynamical point of view. One way to remove these changes is to consider the time evolution of  $\tilde{U}$  rather than of  $U$ :

$$\frac{d\tilde{U}}{dt} = \frac{dU}{dt} - \frac{dU_0}{dt} = (\dots) + \oint z \mathbf{F} \cdot \mathbf{n} d\Gamma - \frac{1}{2} I. \quad (\text{B3})$$

We note that  $\tilde{U}$  is equal to the potential energy referenced to midlevel since  $U'(1/2) = -\langle (z - 1/2) B \rangle = U + \langle B \rangle/2 = \tilde{U}$ . With this reference level, the background potential energy equals zero.

In this study we use a surface buoyancy flux  $F_s(y)$  at the top of the domain and a lateral buoyancy flux  $F_l(z)$  at the southern boundary, so the boundary integral in [Eq. \(18a\)](#) contains two nonzero contributions:

$$\oint z \mathbf{F} \cdot \mathbf{n} d\Gamma = \int_0^1 F_s(y) |_{z=1} dy - \int_0^1 z F_l(z) |_{y=0} dz. \quad (\text{B4})$$

When we separate the fluxes  $F_s$  and  $F_l$  into net components  $I_s$  and  $I_l$ , which must be equal in a steady state, and shape functions  $\tilde{F}_s(y)$  and  $\tilde{F}_l(z)$ , which have zero integral, the surface component of the boundary integral equals

$$\int_0^1 F_s(y) dy = I_s, \quad (\text{B5})$$

whereas the component of the lateral boundary yields an integral denoted by  $K_v$ :

$$\int_0^1 z F_l(z) dz = \frac{1}{2} I_l + \int_0^1 z \tilde{F}_l(z) dz = \frac{1}{2} I_l + K_v. \quad (\text{B6})$$

The resulting expression for the boundary integral now becomes

$$\oint z \mathbf{F} \cdot \mathbf{n} d\Gamma - \frac{1}{2} I = I_s - \frac{1}{2} I_l - K_v - \frac{1}{2} (I_s - I_l)$$

$$= \frac{1}{2} I_s - K_v. \quad (\text{B7})$$

It is interesting to note that the contribution of the boundary integral contains no information on the net lateral buoyancy flux  $I_p$ , but only on the *shape* of the lateral buoyancy flux  $F_l(z)$ . Evidently, a (homogeneously distributed in the vertical) net lateral buoyancy input does not affect the potential energy  $\bar{U}$ , as it only affects the background potential energy  $U_0$ . On the other hand, the surface contribution [Eq. (B5)] contains information on the *net* buoyancy flux only, but not on the shape of the surface buoyancy flux  $F_s(y)$ . Obviously this shape, which accounts for meridional redistribution of buoyancy within a basin, does not directly influence the potential energy of the system.

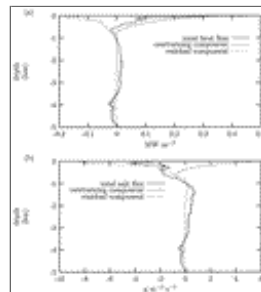
## Tables

Table 1. Symbols and characteristic values of dimensional and nondimensional parameters used in this study.

Parameter	Symbol	Value
Characteristic length scale	$L$	$1 \times 10^7 \text{ m}$
Characteristic depth scale	$H$	$5 \times 10^3 \text{ m}$
Depth of NADW overturning cell	$H_N$	2828 m
Thermal expansivity	$\alpha$	$1.9 \times 10^{-4} \text{ K}^{-1}$
Saline expansivity	$\beta$	$7.6 \times 10^{-4} \text{ psu}^{-1}$
Characteristic temperature range	$\Delta T$	25°C
Characteristic salinity range	$\Delta S$	2 psu
Reference potential temperature	$T_0$	4.83°C
Reference salinity	$S_0$	35.07 psu
Reference density	$\rho_0$	$1 \times 10^3 \text{ kg m}^{-3}$
Gravitational acceleration	$g$	$10 \text{ m s}^{-2}$
Horizontal diffusivity	$\kappa_h$	$1 \times 10^9 \text{ m}^2 \text{ s}^{-1}$
Vertical diffusivity	$\kappa_v$	$1 \times 10^{-4} \text{ m}^2 \text{ s}^{-1}$
Horizontal viscosity	$\nu_h$	$2.25 \times 10^9 \text{ m}^2 \text{ s}^{-1}$
Vertical viscosity	$\nu_v$	$2.25 \times 10^{-4} \text{ m}^2 \text{ s}^{-1}$
Heat capacity	$c_p$	$4 \times 10^3 \text{ J kg}^{-1} \text{ K}^{-1}$
Aspect ratio	$a$	$5 \times 10^{-4}$
Thermal Rayleigh number	Ra	$1 \times 10^4$
Prandtl number	Pr	2.25
Lewis number	Le	1
Buoyancy ratio	$\lambda$	0.32
Amplitude of surface salt flux	$\sigma_s$	0–10
Amplitude of lateral salt flux	$\sigma_l$	0–16
Amplitude of lateral heat flux	$\tau_l$	0–70

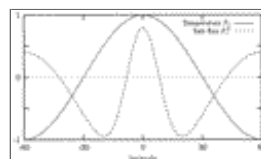
[Click on thumbnail for full-sized image.](#)

## Figures



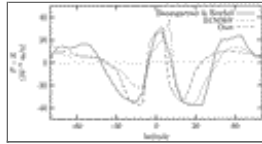
[Click on thumbnail for full-sized image.](#)

Fig. 1. Profiles of meridional advective fluxes of (a) heat (in  $\text{MW m}^{-2}$ ) and of (b) salt (in  $\text{g m}^{-2} \text{ s}^{-1}$ ) across  $30^\circ\text{S}$  in the Atlantic. Solid lines denote the total fluxes, while long-dashed and short-dashed lines denote the overturning and residual components, respectively. Notice the large southward contributions of the gyre-induced residual fluxes in the upper 1000 m, and the northward heat and salt fluxes at NADW level. Data used are from an inversion of WOCE data performed by J. Holfort (IfM, Kiel, Germany).



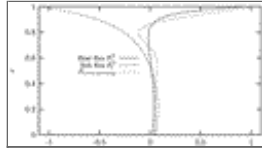
[Click on thumbnail for full-sized image.](#)

Fig. 2. Profiles of prescribed surface temperature  $T_s$  and surface salt flux  $F_s^S$  as a function of latitude.



[Click on thumbnail for full-sized image.](#)

Fig. 3. Profiles of  $P - E$  (in  $10^{-9} \text{ m s}^{-1}$ ) for the three different datasets as indicated in the figure.



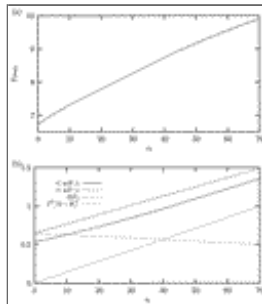
[Click on thumbnail for full-sized image.](#)

Fig. 4. Profiles of prescribed lateral heat ( $F_l^T$ ) and salt ( $F_l^S$ ) fluxes. The overturning salt flux profile  $F_{l,\text{overturning}}$  is used in the discussion.



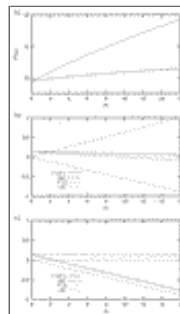
[Click on thumbnail for full-sized image.](#)

Fig. 5. Streamfunction profiles of NPP states at  $\sigma_s = 16.0$  in the (a) global domain north of  $30^\circ\text{S}$ , and (b) its Atlantic domain counterpart. At the southern boundary of the latter state fluxes of heat and salt are prescribed, which are diagnosed at  $y = 0.25$  in the global state. Streamfunction is scaled with the maximum of the Atlantic state in both panels. Solid contours denote clockwise circulation (negative  $\psi$ ), and have an increment of 0.2.



[Click on thumbnail for full-sized image.](#)

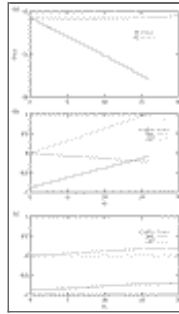
Fig. 6. Relations between lateral heat flux amplitude  $\tau_l$  and (a) overturning strength  $\psi_{\text{max}}$ , and (b) buoyancy production  $\langle wB \rangle$  and its thermal component  $\langle wT \rangle$ . In steady state,  $\langle wT \rangle$  equals the sum of the vertical temperature difference  $\Delta T_{\text{v}}$  and the boundary flux contribution  $I^T/2 - K^T_{\text{v}}$ . The lateral heat flux  $F_l^T$  is plotted in [Fig. 4](#) (solid line) and given by [Eq. \(11a\)](#). The value  $\tau_l = 70$  is representative for observed fluxes across  $30^\circ\text{S}$  [[Eq. \(12\)](#)].



[Click on thumbnail for full-sized image.](#)

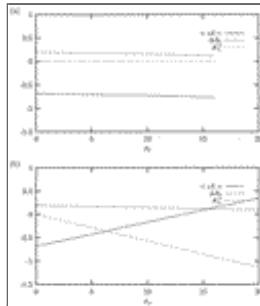
Fig. 7. (a) Relation between the lateral salt flux amplitude  $\sigma_l$  and overturning strength  $\psi_{\text{max}}$ , for a lateral salt flux with vertical

profile  $F_l^S$  (solid line) and for a vertically uniform lateral salt flux (dashed line). (b), (c) Relation between the lateral salt flux amplitude  $\sigma_l$  and the saline component  $\langle wS \rangle$  of the buoyancy production for the vertical profile case (b) and for the vertically uniform case (c). In steady state,  $\langle wS \rangle$  equals the sum of the vertical salinity difference  $\Delta S_v$  and the boundary flux contributions  $\dot{I}^S/2 - K^S_v$ . The flux profile  $F_l^S$  is plotted in Fig. 4 (long-dashed line) and given by Eq. (11b). The value  $\sigma_l = 16$  is representative for observed fluxes across 30°S [Eq. (13)]. Note that  $\langle wB \rangle \propto -\langle wS \rangle$ , so a positive value of  $\langle wS \rangle$  tends to brake the flow.



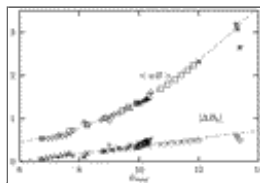
Click on thumbnail for full-sized image.

Fig. 8. (a) Overturning strength  $\psi_{\max}$  as a function of lateral salt flux amplitude  $\sigma_l$  (solid line) and surface salt flux amplitude  $\sigma_s$  (dashed line). The net flux was kept fixed, and only the amplitudes of the profiles were changed. In (b) and (c) the relevant terms in the buoyancy production are plotted for both cases, showing that the shape of the lateral flux contributes directly to the energy balance through  $-K^S_v$  while the shape of the surface salt flux only influences the energy balance in an indirect way through  $\Delta S_v$ .



Click on thumbnail for full-sized image.

Fig. 9. The relevant terms in the balance of the buoyancy torque [Eq. (24a)] for the same cases as in Fig. 8. The increase in the lateral flux (a) has almost no impact on this balance, whereas the increase in the surface flux (b) causes the change in  $K^S_h$ . This change is balanced by the advection term  $\langle \mathbf{U}S \rangle$  rather than by the meridional salinity difference  $\Delta S_h$ .



Click on thumbnail for full-sized image.

Fig. 10. Plot of  $\langle wB \rangle$  and  $\Delta B_h$  vs  $\psi_{\max}$  for all experiments performed. Curves are best-fit quadratic ( $\langle wB \rangle$ ) and linear ( $\Delta B_h$ ) functions.





Click on thumbnail for full-sized image.

Fig. 11. Saline component of the buoyancy production  $\langle wS \rangle$  and its components as a function of the parameter  $\mu$ , where  $\mu = 0$  denotes the model with the total salt flux prescribed, whereas at  $\mu = 1$  the zonally averaged overturning component is prescribed (see Fig. 4). Note that an increase in  $\langle wS \rangle$  corresponds to an increase in the weakening effect of salinity on the circulation strength (a decrease in  $\langle wB \rangle$ ).

Corresponding author address: Wilbert Weijer, Institute for Marine and Atmospheric Research Utrecht, Utrecht University, Princetonplein 5, 3584 CC Utrecht, the Netherlands.

E-mail: [weijer@phys.uu.nl](mailto:weijer@phys.uu.nl).

top ▲



© 2008 American Meteorological Society [Privacy Policy and Disclaimer](#)  
Headquarters: 45 Beacon Street Boston, MA 02108-3693  
DC Office: 1120 G Street, NW, Suite 800 Washington DC, 20005-3826  
[amsinfo@ametsoc.org](mailto:amsinfo@ametsoc.org) Phone: 617-227-2425 Fax: 617-742-8718  
[Allen Press, Inc.](#) assists in the online publication of AMS journals.